ARTICLE

Self-Assembly of Peptides into Spherical Nanoparticles for Delivery of Hydrophilic Moieties to the Cytosol

Louise Collins,[†,⊥] Alan L. Parker,[†,⊥] John D. Gehman,[‡,⊥] Lorna Eckley,[†] Matthew A. Perugini,[§] Frances Separovic,[‡] and John W. Fabre[†,*]

[†]Department of Clinical Sciences, King's College London School of Medicine, James Black Centre, 125 Coldharbour Lane, London, SE5 9NU England, [‡]School of Chemistry, Bio21 Institute, University of Melbourne, Melbourne VIC 3010, Australia, and [§]Department of Biochemistry and Molecular Biology, Bio21 Molecular Science and Biotechnology Institute, University of Melbourne, Victoria 3010, Australia. [⊥]These authors contributed equally to this work.

ABSTRACT We report a novel class of self-assembling peptide nanoparticles formed by mixing aqueous solutions of K_{16} peptide and a 20 amino acid peptide of net charge −5 (GLFEALLELLESLWELLLEA). Particle formation is salt-dependent and yields perfectly spherical nanoparticles of ~120 to ~800 nm diameter, depending on buffer composition and temperature, with a stoichiometry of ~1:2.5 for the cationic and anionic peptides. The anionic peptide forms an α-helix in aqueous solution, has all five glutamates on one side of the helix, and exists entirely as a discrete oligomer of 9−10 peptides. A rigid oligomer with 45−50 negative charges almost certainly represents the core component of these nanoparticles, held together by electrostatic interactions with the unstructured K_{16} peptide. Cells internalize these particles by an endocytic process, and free particles are frequently seen in the cytosol, presumably because of the acid-dependent fusogenic properties of the anionic peptide. Among other applications, these particles have potential for the targeted delivery of single or multiple therapeutic moieties directly to the cytosol, and we report the successful delivery of a K_{16}-linked pro-apoptosis peptide.

KEYWORDS: peptides · nanoparticles · fusogenic peptide · drug delivery

The properties of monomeric components that self-assemble into nanoparticles vary widely[1−5] and include oppositely charged macromolecular components.[6−8] In general, small synthetic peptides do not adopt secondary structures in aqueous solution and are unlikely candidates as building blocks for particle formation. However, synthetic peptides which are charge self-complementary have been designed to form β-sheets with distinct polar and nonpolar surfaces, and these self-assemble into nanofibers.[9] We have previously reported that a 20 amino acid anionic peptide (GLFEALLELLESLWELLLEA) unexpectedly forms an α-helix in aqueous solution.[10] This peptide is based on the fusogenic region of influenza virus hemagglutinin[11,12] and, because of its acid-dependent fusogenic properties, has been used to effect endocytic exit of DNA plasmids from endocytic vesicles.[10,13,14] We examined a solution of K_{16} peptide and the anionic fusogenic peptide by dynamic light scattering (DLS) and found that the two peptides alone (without DNA plasmids) formed excellent particles. This unexpected observation was the basis for this study.

The delivery to the cytosol of membrane-impermeable substances (such as biologically active peptides and proteins) could have wide-ranging experimental and clinical applications and would represent a novel approach to therapeutics. "Cell-penetrating" peptides are small, usually arginine-rich peptides, which occur either as natural sequences (*e.g.*, in the TAT protein of human immunodeficiency virus type-1)[15] or as synthetic polyarginines.[16] They were originally considered to translocate directly across the plasma membrane and have been extensively investigated.[17−19] Such peptides, and the cargo molecules to which they are attached, are now believed to be internalized by endocytosis.[20,21]

The peptide nanoparticles described in this paper represent an alternative approach, specifically targeted for delivery to the cytosol *via* the endocytic pathway. From a structural point of view, they represent a novel class of nanoparticle based on a rigid core with high multiple charges of one type and flexible unstructured linking molecules of opposite charge. From a therapeutic point of view, they offer the possibility of carrying multiple components in predetermined proportions to the cytosol, including both cellular targeting and biologically active compounds.

RESULTS AND DISCUSSION

Initial Studies. Particle formation was initially discovered when the K_{16} peptide at

*Address correspondence to john.fabre@kcl.ac.uk.

Received for review October 14, 2009 and accepted April 13, 2010.

Published online April 21, 2010. 10.1021/nn901414q

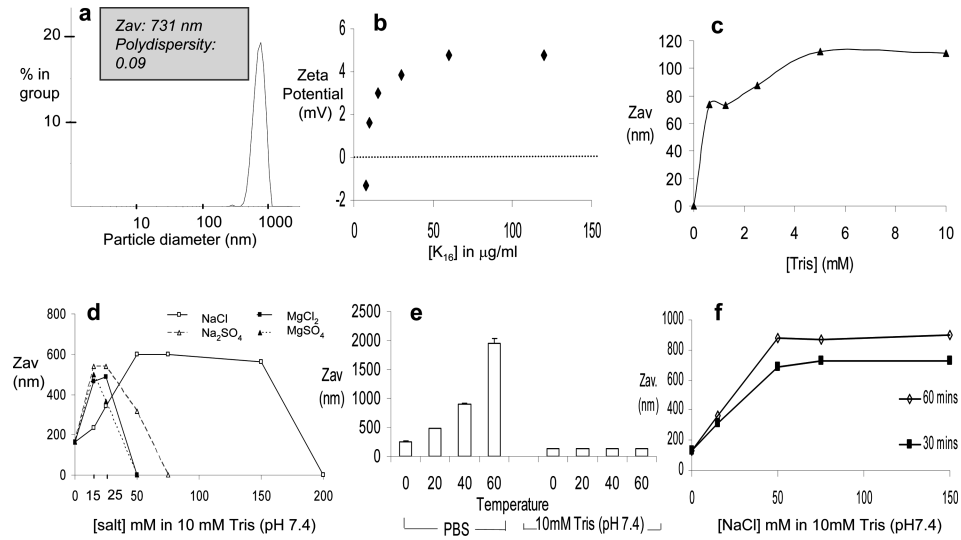

Figure 1. Particle formation by K_{16} peptides and the anionic GLFEALLELLESLWELLLEA peptide. (a) Dynamic light scattering. A solution of the K_{16} peptide at 15 μg/mL (3.7 μM) and the fusogenic peptide at 10 μg/mL (4.1 μM) (± charge ratio of 2.9:1) in phosphate buffered saline (PBS) was examined 30 min after mixing the peptides. A uniform population of particles with low polydispersity is produced. Solutions of the K_{16} peptide alone and the fusogenic peptide alone do not have any particles. (b) Zeta potential of particles formed in 0.15 M NaCl, 10 mM Tris, pH 7.4 with the fusogenic peptide at a constant 10 μg/mL (4.1 μM) and the K_{16} peptide (from left to right on the graph) at 7.5, 10, 15, 30, 60, and 120 μg/mL (1.9−30.0 μM) (± charge ratios of 1.4 to 23.4). (c,d) Influence of salt. (c) Dynamic light scattering was performed 30 min after mixing the fusogenic peptide at 10 μg/mL and the K_{16} peptide at 15 μg/mL in pure water (zero point) or in dilutions in water of 10 mM Tris, pH 7.4. (d) K_{16} peptide at 15 μg/mL and fusogenic peptide at 10 μg/mL were mixed in 10 mM Tris, pH 7.4, with various concentrations of salts, as indicated. After 30 min, Z_{av} was determined by dynamic light scattering. At 25 mM $MgSO_4$ and 50 mM Na_2SO_4, particles were smaller and fewer events were recorded (63 and 67 kilocounts per second, normally >100 kilocounts per second). (e) Influence of temperature. The K_{16} peptide at 15 μg/mL and fusogenic peptide at 10 μg/mL in either PBS or 10 mM Tris were mixed and maintained at the temperatures indicated. After 30 min, Z_{av} was determined by dynamic light scattering. (f) Influence time. Dynamic light scattering was performed 30 and 60 min after mixing the fusogenic peptide at 10 μg/mL and the K_{16} peptide at 15 μg/mL in 10 mM Tris, pH 7.4, with NaCl at the concentrations indicated.

15 μg/mL (3.7 μM) was mixed with the fusogenic peptide at 10 μg/mL (4.1 μM) in phosphate buffered saline (PBS). This yielded a uniform population of particles with Z_{av} = 731 nm (Figure 1a). Both peptides are soluble in pH-neutral aqueous solutions, and neither alone has any particles in solution. Particle formation was evaluated with the fusogenic peptide at constant 10 μg/mL and the K_{16} peptide at a range of concentrations from 3.75 to 240 μg/mL (0.9−60.0 μM) in PBS. No particles were formed with K_{16} at 3.75 μg/mL, which represents an excess of negative charges in the peptide mix (± charge ratio 1:1.4). Particles were formed at all other K_{16} concentrations and were larger as the K_{16} concentration increased (Z_{av} range ~400 to ~900 nm at 30 min) (Supporting Information Figure 1). The surface charge of the particles increased with each increase in the K_{16} concentration, up to 60 μg/mL (Figure 1b). It is noteworthy that particles formed with 7.5 μg/mL K_{16} had a negative surface charge, although the ± charge ratio of the peptide mix was 1.4:1, which will be discussed under stoichiometry below.

Importance of Charge Shielding for Particle Formation. As electrostatic interactions are presumably involved in particle formation, we investigated the role of salt ions in particle formation. No particles were formed with peptides in pure water (Figure 1c, zero point), suggesting a role for salt ions in charge shielding during particle formation. Particles in 10 mM Tris, pH 7.4, were much smaller (Z_{av} ~100−150 nm) than in PBS and became progressively smaller in dilutions of 10 mM Tris (Figure 1c). Addition of salt promoted particle formation, but at high salt concentrations, the particles dissociated. At 15 mM NaCl, the Z_{av} was 234 nm, while 15 mM $MgCl_2$, Na_2SO_4, and $MgSO_4$ gave Z_{av} values of 466, 541, and 499 nm, respectively (Figure 1d). Increasing NaCl concentration resulted in increasing particle size up to a plateau Z_{av} of ~600 nm at 50−150 mM NaCl. However, 200 mM NaCl completely abolished particle formation, presumably because of competition between salt ions and interpeptide salt bridges. Particle formation was inhibited or abolished at lower ionic strengths of the divalent cations: 50 mM Na_2SO_4, 50 mM $MgCl_2$, and 25 mM $MgSO_4$.

In the absence of salt, particles in 10 mM Tris, pH 7.4, are resistant to temperature-induced increase in size, whereas in PBS, particle size at 30 min increases ~10-fold over 0−60 °C (Figure 1e). Similarly, particle size is stable with time in the absence of salt, but in the presence of salt, it increases slowly with time, for example, from Z_{av} of 731 nm to Z_{av} of 904 nm over 30−60 min in 150 mM NaCl (Figure 1f).

Controlling Particle Size and Charge. Small, electrically neutral particles are likely to be optimal for therapeutic purposes, both for biodistribution and for cellular uptake by specific cell surface receptors. We evaluated the use of HPMA to control particle size and reduce sur-

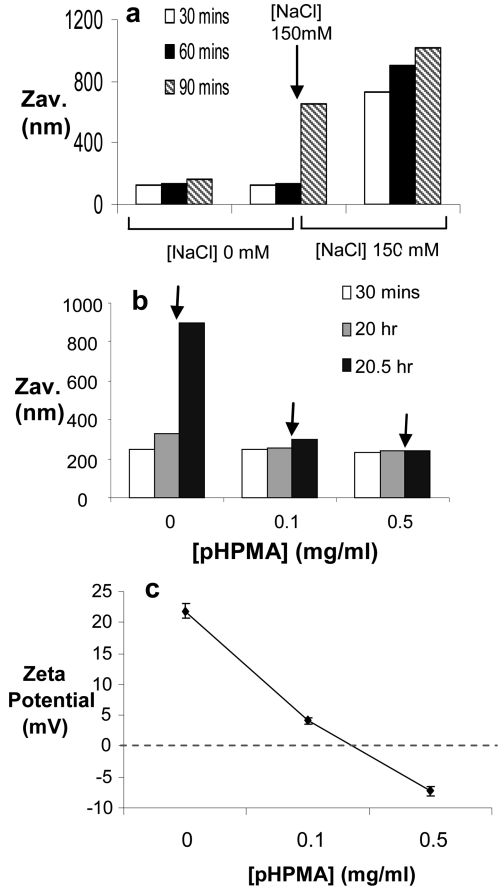

Figure 2. Particle charge and stability. (a) Salt-induced particle growth. Dynamic light scattering was performed at the times indicated after mixing the K_{16} peptide at 15 μg/mL and the fusogenic peptide at 10 μg/mL, either in the absence of NaCl (group on left) or in 150 mM NaCl (group on right). In the middle group, the NaCl concentration was increased from 0 to 150 mM at 60 min. (b) Polymer coating and particle stability. The K_{16} peptide at 15 μg/mL and the fusogenic peptide at 10 μg/mL were mixed in 10 mM NaCl, 20 mM Hepes, pH 7.8. HPMA was added after 30 min to 0.1 or 0.5 mg/mL. Dynamic light scattering was performed at 30 min, 20 h, and 20.5 h after addition of HPMA, as indicated. At 20 h, as marked by the arrow, the NaCl concentration was increased to 150 mM. (c) Polymer coating and particle charge. The K_{16} peptide at 15 μg/mL and the fusogenic peptide at 10 μg/mL were mixed in 20 mM Hepes, pH 7.8. HPMA was added after 30 min at 0.1 or 0.5 mg/mL, as indicated. Zeta potential was measured at 20 h.

face charge. The nitrophenol group of HPMA targets and, of particular importance, neutralizes exposed NH_3^+ groups. The HPMA used in these studies has ~14 nitrophenol groups per molecule, and it would therefore make multipoint attachments to the particle surface.

If particles are formed in the absence of salt, and then NaCl is added at 60 min, particle size increases dramatically to that normally seen with NaCl (Figure 2a). HPMA-treated particles were resistant to salt-induced increase in size (Figure 2b) and showed a progressive decrease of surface positive charge with increasing HPMA concentration (Figure 2c). Whether or not HPMA coating will affect the functional components of the nanoparticles remains to be established.

Stoichiometry of Peptides within Particles. Stoichiometry was calculated by measuring peptide concentration after removal of particles by centrifugation. The molar ratio of K_{16} to fusogenic peptide within the particles was ~1:2.5, irrespective of buffer composition and initial peptide ratio (Supporting Information Table 1). This represents an excess of positive charge by a factor of ~1.3 within the particle, indicating that not all NH_3^+ groups of lysines are involved in interpeptide salt bridges. A net uptake of salt anions into the particle would therefore be expected during the initial phase of particle formation to neutralize excess NH_3^+ groups within the particle and maintain an electrically neutral core. This is consistent with the dependence of particle formation on the presence of salt.

When peptides are mixed at approximately the same molar ratio as in the particle core, the surface charge of the particle is negative (*e.g.*, with K_{16} at 7.5 μg/mL in Figure 1b). This suggests the presence of exposed fusogenic peptide oligomers on the particle surface at this minimal K_{16} to fusogenic peptide ratio. As K_{16} is supplied in increasing excess, the exposed anionic groups on the particle surface absorb more K_{16} peptide until they saturate at ~60 μg/mL (Figure 1b).

Particle Formation with Peptide Homologues. We wished to establish any structural constraints on particle formation and, in particular, to evaluate the possibility of linking functional moieties to the peptide constituents of the particles. We therefore evaluated several peptides containing 16 lysines for particle formation with the fusogenic peptide (Table 1). Interestingly, alternating lysine residues in $(K-H)_{16}$ (row 3) formed excellent particles, but $(K-P)_{16}$ (row 4) did not. The α-nitrogen of proline is covalently linked to its side chain, which limits the rotational freedom of the lysine−proline bond. An unstructured cationic peptide might be required for the NH_3^+ groups to accommodate optimally the CO_2^- groups on the rigid fusogenic peptide oligomer. $K_{16}H_{16}$ (row 5) gave high particle counts, similar to K_{16} and $(K-H)_{16}$, but the particles were much larger and diverse in size. This is possibly because H_{16} represents a potentially highly hydrophobic sequence, depending on the pK_a of the imidazole groups in the peptide (6.0 for free histidine). Rows 6−11 involve the minimal peptide sequence for binding to the serpin−enzyme complex receptor[22] and demonstrate particle formation down to K_6, although polydispersity is better with K_8. Long polylysine chains (>100 lysines) (row 12) form excellent particles. Cyclized and linear peptides of 30 or 31 amino acids, comprising K_{16} at the amino terminus with various integrin-binding moieties,[23−26] or a 17 amino acid sequence targeting the serpin−enzyme complex receptor,[22] all formed excellent particles (rows 13−17). K_{16} with a pro-apoptosis peptide[27] also gave excellent particles (row 18).

Higher Order Structure of the Anionic Fusogenic Peptide. We have previously reported that the fusogenic peptide

TABLE 1. Particle Formation by K_{16} and Fusogenic Peptide Homologues

	cationic peptide[a]	anionic peptide	Z_{av} (nm)	polydispersity
1	K_{16}	GLFEALLELLESLWELLLEA[b]	605	0.20
2	K_{16}	AAAEAAAEAAEAAAEAAAEA[c]	no particles	
3	$(KH)_{16}$	GLFEALLELLESLWELLLEA	654	0.01
4	$(KP)_{16}$	GLFEALLELLESLWELLLEA	no particles	
5	$K_{16}(H)_{16}$	GLFEALLELLESLWELLLEA	1178	1.00
6	K_{16}-FNKPFVFLI[d]	GLFEALLELLESLWELLLEA	1064	0.28
7	K_{12}-FNKPFVFLI	GLFEALLELLESLWELLLEA	1164	0.14
8	K_8-FNKPFVFLI	GLFEALLELLESLWELLLEA	709	0.19
9	K_6-FNKPFVFLI	GLFEALLELLESLWELLLEA	756	0.84
10	K_4-FNKPFVFLI	GLFEALLELLESLWELLLEA	no particles	
11	K_2-FNKPFVFLI	GLFEALLELLESLWELLLEA	no particles	
12	polylysine[e]	GLFEALLELLESLWELLLEA	682	0.12
13	K_{16}-ICRRARGDNPDDRCT[f]	GLFEALLELLESLWELLLEA	726	0.14
14	K_{16}-IGRRARGDNPDDRGT[g]	GLFEALLELLESLWELLLEA	672	0.12
15	K_{16}-ICRRARGENPDDRCT[h]	GLFEALLELLESLWELLLEA	630	0.02
16	K_{16}-CPPASYRGDSCQE[i]	GLFEALLELLESLWELLLEA	697	0.18
17	K_{16}-CSIPPEVKFNKPFVFLI[j]	GLFEALLELLESLWELLLEA	822	0.32
18	K_{16}-PVKRRLFG[k]	GLFEALLELLESLWELLLEA	669	0.07

[a]Cationic peptides were at 15 μg/mL and the anionic peptides at 10 μg/mL in PBS. Z_{av} was measured 30 minutes after mixing the peptides. [b]Fusogenic peptide, based on influenza virus hemagglutinin.[13] Note that all amino acids are hydrophobic except for 5 glutamates. [c]Fusogenic peptide homologue. All amino acids except glutamates have been replaced with alanines. [d]Rows 6−11. K_{16} to K_2 with a shortened version of the human α1-antitrypsin sequence.[22] [e]Commercial polylysine, 100−200 lysines per chain (Sigma-Aldrich, Cat. No. P7890). [f]K_{16} with cyclized peptide containing the 15 amino acid integrin-binding loop from the snake venom molossin.[23,24] [g]K_{16} with noncyclized version of the molossin peptide (see row 13), with the cysteine residues replaced by glycines. [h]K_{16} with cyclized peptide homologous to the molossin peptide (see row 13), with the integrin-binding RGD motif replaced by RGE.[25] [i]K_{16} with cyclized peptide containing the 14 amino acid integrin-binding loop of human laminin.[26] [j]K_{16} with human α1-antitrypsin sequence which binds to the serpin−enzyme complex receptor.[22] [k]K_{16} with a pro-apoptotic peptide.[27]

forms an α-helix in aqueous solution[10] (Figure 3a). However, the alanine homologue (AAAEAAAEAAEAAAEAAAEA), which does not form particles (Table 1, row 2), is a random coil (Figure 3a). Modeling the fusogenic peptide as an α-helix shows that all negative charges are on one side of the helix (Figure 3b). Thus, the peptide adopts a rigid, rod-like structure, with one hydrophilic face. Analytical ultracentrifugation was performed to look for a higher order structure. Sedimentation velocity data for 50, 250, and 700 μg/mL peptide indicated a single, monodisperse molecular mass of 22.485 kDa (Figure 3c−e). Sedimentation equilibrium data at 1 mg/mL peptide (Figure 3f), together with sedimentation velocity data, indicated a molecular mass of 21.849 ± 0.043 kDa. These data suggest a structural model where the fusogenic peptide self-assembles *via* hydrophobic packing into a relatively rigid oligomer of 9 or 10 peptides (calculated molecular masses 20.715 and 23.017 kDa, respectively) with 45−50 negative surface charges.

Visualization of Particle. In order to visualize the particles in their native state in aqueous solution, and also to evaluate their interaction with cells, a cell line was incubated with gold-labeled peptide nanoparticles for 4 h and then fixed for electron microscopy. Figure 4a shows a perfectly spherical particle in the extracellular fluid. Figure 4a also shows a particle inside the cell not enclosed by a membrane. Many intracellular particles were membrane-enclosed (Figure 4b). This suggests internalization by macropinocytosis followed by dissolution of the endocytic membrane. Initial attachment of the particle to the plasma membrane is probably by electrostatic interactions.

Functional Studies. The presence of free particles in the cytosol suggests that routing therapeutic peptide particles *via* the endocytic pathway to the cytosol is an interesting possibility. To evaluate delivery of a biologically active moiety, the PVKRRLFG apoptosis-inducing peptide[27] was chosen. Figure 4c shows that PVKRRLFG alone, K_{16}PVKRRLFG alone, and K_{16}PVKRRLFG with the alanine homologue of the fusogenic peptide did not induce apoptosis. Control particles formed with K_{16} plus the fusogenic peptide also were without effect. However, particles formed with K_{16}-PVKRRLFG and the fusogenic peptide induced apoptosis as effectively as the positive control, staurosporine.

Nucleation of Particle Formation. The initial phase of particle formation involves consumption of the fusogenic peptide to form particles of constant stoichiometry, leaving free K_{16}. This phase is complete by 30 min (Supporting Information Table 1). We formed particles with K_{16} at 15 or 120 μg/mL, and then added fresh fusogenic peptide at 28 min. In the absence of fresh fusogenic peptide, there was (as expected) a single population of particles at 30 min (Supporting Information Figure 2a). The addition of fresh fusogenic peptide at 28 min resulted in two populations of particles at 30 min (2 min after addition of fresh fusogenic peptide), one presumptively of newly formed small particles (peak 307 nm) and the other presumptively the pre-existing particles, but larger (peak 875 nm) than in the absence of fresh fusogenic peptide (peak 574 nm) (Supporting In-

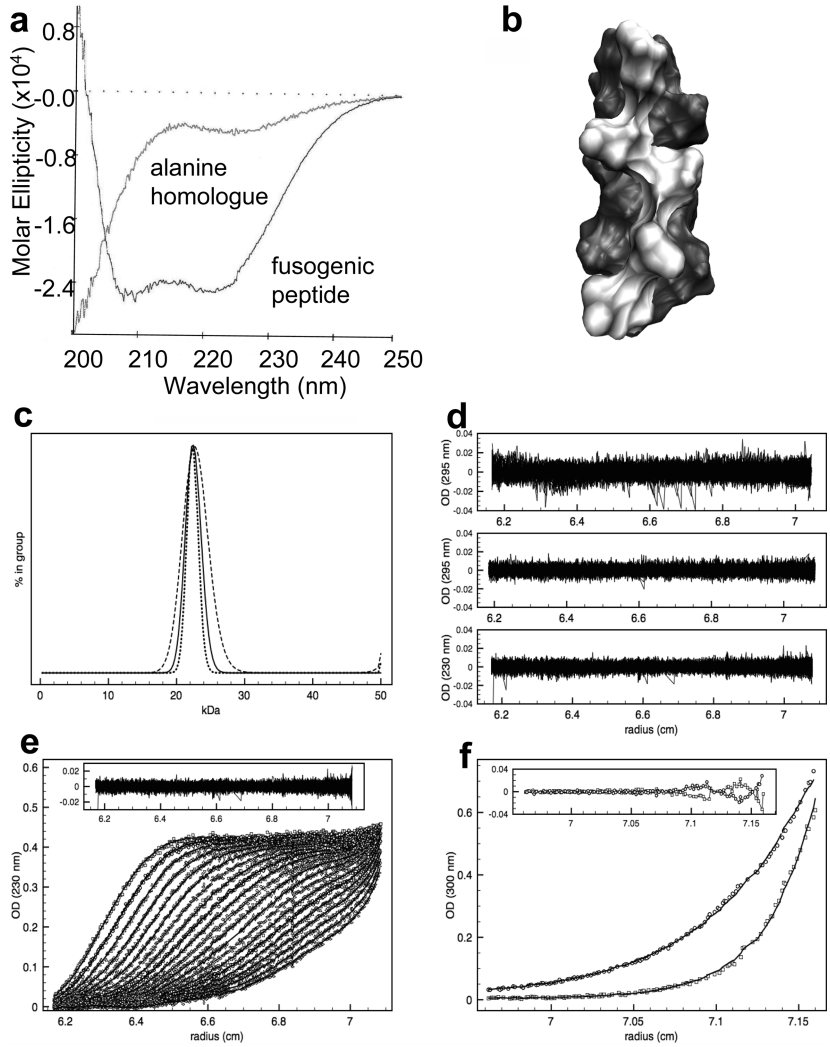

Figure 3. Structural studies on the fusogenic peptide. (a) Circular dichroism studies. The fusogenic peptide (Table 1, row 1) and the alanine homologue of the fusogenic peptide (Table 1, row 2) are shown. On the basis of model secondary structures from Gratzer *et al.*,[31] the fusogenic peptide shows an α-helix conformation, while the alanine homologue corresponds to a random coil. (b) Distribution of negative charges (white area) on the surface of an α-helical model of the fusogenic peptide. The peptide backbone was folded into a canonical α-helix (dihedral angles ψ,φ,ω = −62,−41,180), and side chain conformational energy was minimized using molecular dynamics in VMD[35] and the companion NAMD[36] software utilities while the backbone was held constant. (c) Molecular weight distributions fit individually to sedimentation velocity experiments for 50 (solid line), 250 (dashed line), and 700 (dotted line) μg/mL fusogenic peptide concentrations. All distributions are maximum at a molecular mass of 22.485 kDa. (d) Residuals between sedimentation velocity data and distribution fits shown in (c) for 50, 250, and 700 μg/mL fusogenic peptide in the bottom, middle, and top panels, respectively. Root mean square deviations (rmsd) between the data and the fits are 0.004, 0.004, and 0.006, and the runs test *Z* (a measure of the randomness of the residuals, where smaller values indicate less systematic error)[37] are 8.9, 5.1, and 30.0 for 50, 250, and 700 μg/mL fusogenic peptide, respectively. (e) Data (symbols), fits (lines), and residuals (inset) of the global analysis incorporating all sedimentation velocity and equilibrium data. Every third scan of the 50 μg/mL is shown; fits to sedimentation velocity data for other time points as well as 250 and 700 μg/mL fusogenic peptide concentrations are similar. (f) Data for 35k rpm (circles) and 50k rpm (squares) sedimentation equilibrium experiments with global analysis fits (lines) and residuals (inset).

formation **Figure 2b). By 45 min, the two populations had merged (Supporting Information Figure 2c).**

The standard procedure for particle formation involves adding fusogenic peptide at 1 mg/mL to K_{16} at 15 μg/mL, which gives particles of Z_{av} 623 nm, peak 698 nm (Supporting Information Figure 2d). Interestingly, adding K_{16} at 1 mg/mL to the fusogenic peptide at 10 μg/mL (Z_{av} 336 nm, peak 297 nm) (Supporting Information Figure 2e), or mixing equal volumes of K_{16} at 30 μg/mL and fusogenic peptide at 20 μg/mL (Z_{av} 364 nm, peak 361 nm) (Supporting Information Figure 2f) gave smaller particles. Thus, local high concentrations of fusogenic peptide favor particle formation.

Nanoparticles of the nature described in this paper have not previously been reported. They might form the prototype for a new class of self-assembled particle that employs rigid molecules of high net surface charge as the core building block, with unstructured polymers of opposite charge to tether them together ("bricks and straps" hypothesis, Figure 5). These particles could have wide applications, both in biological and nonbiological systems. For

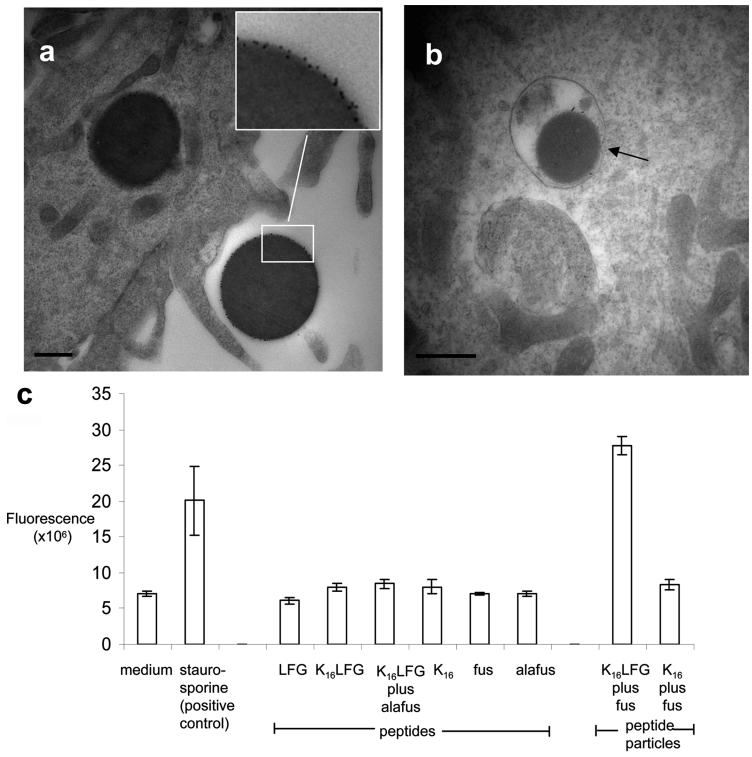

Figure 4. Ultrastructural and functional studies. (a,b) Transmission electron microscopy. The K_{16}-molossin peptide (Table 1, row 13) (carrying a biotin molecule on the amino terminal lysine) at 15 μg/mL (2.4 μM) and the fusogenic peptide at 10 μg/mL (4.1 μM) (± charge ratio of 1.9:1) were allowed to stand for 30 min before addition of streptavidin−gold. The gold-labeled particles were added to T-24 cells, and the cells were harvested 4 h later. (a) Perfectly spherical gold-labeled particle can be seen in the extracellular fluid, close to the plasma membrane. The particle inside the cell has a less electron-dense halo, and the endocytic membrane has been completely disrupted. (b) Particle within an endocytic vesicle is shown. The endocytic membrane closest to the particle appears less dense than the rest of the endocytic membrane, and at one point (arrowed), the endocytic membrane is indented to the surface of the particle. The bars in a and b are 500 nm. The particles observed are large (>1000 nm) because of the long time (4.5 h) between particle formation and assay. (c) Apoptosis study. U2-OS osteosarcoma cells were exposed for 4 h to 1 μM staurosporine, PVKRRLFG (LFG) peptide (4 μg/mL, 2.9 μM), K_{16} PVKRRLFG (K_{16}LFG) peptide (9 μg/mL, 1.6 μM), K_{16} PVKRRLFG at 9 μg/mL plus the alanine homologue of the fusogenic peptide at 10 μg/mL, K_{16} peptide (8 μg/mL, 2 μM), fusogenic peptide (fus) (10 μg/mL), the alanine homologue of the fusogenic peptide (alafus) (10 μg/mL), K_{16} PVKRRLFG (9 μg/mL) plus fusogenic peptide (10 μg/mL), and K_{16} (8 μg/mL) plus fusogenic peptide (10 μg/mL). Where two peptides were used, they were mixed and then added to the cells 30 min after mixing. All peptides were in McCoys 5A medium. Note that K_{16}LFG plus alafus (Table 1, row 2) does not form particles. After the 4 h incubation, 100 μg/mL of Apo-ONE homogeneous caspase-3/7 assay substrate (Promega) was added. After 1 h, fluorescence was measured. Note that 8 μg/mL of K_{16} was chosen for particle formation in order to form particles that were neutral or had a negative charge (see Figure 1b), as cationic particles gave background apoptosis. K_{16} PVKRRLFG at 9 μg/mL has a similar number of positive charges as K_{16} at 8 μg/mL. The PVKRRLFG peptide at 20 μg/mL (14.5 μM) gave results similar to 4 μg/mL. Staurosporine showed very little variation in apoptosis levels between 1 and 10 μM concentrations.

example, the particles described in this paper incorporate an acid-dependent fusogenic peptide and might provide a versatile system for the targeted delivery to the cytosol of biologically active, hydrophilic compounds. Alternatively, if the anionic component is formed from peptides that lack fusogenic properties, the particles could be targeted for transcytosis or for delivery to the lysosomal compartment.

Particle formation is almost certainly a consequence of the unusual properties of the anionic fusogenic peptide. This forms an amphipathic α-helix and then oligomerizes, probably by hydrophobic interactions, into a nonamer or a decamer. On addition of the unstructured K_{16} peptide, electrostatic interactions between the NH_3^+ groups and the CO_2^- groups on the polyanionic oligomer initiate particle formation. Probably because the apposition of NH_3^+ and CO_2^- groups on the peptides is not perfect, particle formation requires salt to shield the unpaired charged groups on the peptides. The initial phase of particle formation involves consumption of the anionic peptide to a constant stoichiometry and is complete before 30 min (Supporting Information Table 1). Thereafter, particle growth probably occurs by collision-based exchange of material or particle merger. The influence of salt on this phase of particle growth is probably a consequence of the fact that it drastically reduces surface charge (compare zeta potentials in Figure 1b and Figure 2c).

A particular advantage of these particles is that it should be possible to include multiple functional components in predetermined proportions, for example, for targeting to particular plasma membrane receptors

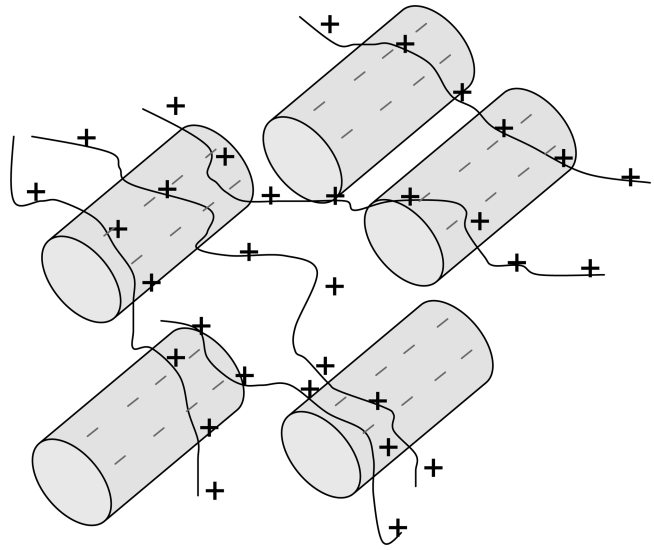

Figure 5. Model of "bricks and straps" hypothesis. Diagrammatic representation of the rigid anionic oligomers of the fusogenic peptide as the bricks and K_{16} chains as the unstructured cationic straps. The nanoparticle would be formed by the random linking of peptide oligomers, by electrostatic interactions between NH_3^+ and CO_2^- groups, with salt ions associating with any unpaired NH_3^+ and CO_2^- groups on the peptides.

and for single or multiple steps in biological processes. In addition, as the interior of the particle is likely to be largely water-excluding, it might be possible to incorporate moieties sensitive to enzymatic or chemical modification (*e.g.*, hydrolysis, oxidation) as labile groups are likely to be protected in the peptide core.

MATERIALS AND METHODS

Peptides. The 17 cationic and two anionic peptides (listed in Table 1) were synthesized, cyclized *via* cysteines (where indicated), and purified by Cambridge Research Biochemical (Cleveland, UK). They were supplied as trifluoroacetate (TFA) salts in the form of a dry powder and stored desiccated at −35 °C. There is one TFA counterion for each positive charge in the peptide. Quantities of 1−2 mg were dissolved at 1 mg/mL in PBS (137 mM NaCl, 1.5 mM KH_2PO_4, 8.1 mM Na_2HPO_4, 2.7 mM KCl, 0.9 mM $CaCl_2 \cdot 2H_2O$, 0.5 mM $MgCl_2 \cdot 6H_2O$, pH 7.4) (Sigma-Aldrich, Dorset, UK); 150 mM NaCl, 10 mM Tris, pH 7.4; 10 mM Tris, pH 7.4, without salt; or 10 mM NaCl, 20 mM Hepes, pH 7.8 (which does not have primary amines) and stored in aliquots at −35 °C. The K_{16}-molossin peptide (Table 1, row 13) was additionally synthesized with a biotinylated lysine at the amino terminus. The high molecular weight polylysine (Table 1, row 12) was from Sigma-Aldrich (Dorset, UK).

Formation of Peptide Particles. The standard conditions involved diluting the K_{16} peptide to 15 μg/mL (3.7 μM) in PBS and then adding the required volume of fusogenic peptide (Table 1, row 1) at 1 mg/mL in PBS to give a concentration of 10 μg/mL (4.1 μM), while constantly stirring. This represents a ± charge ratio of 2.9:1. After 30 min at room temperature, the solution was analyzed. The standard conditions were varied, as indicated in the text, in order to evaluate homologous peptides, peptide concentration, salt concentration, and the influence of time and surface modification.

Analysis of Particle Size by Dynamic Light Scattering (DLS). DLS measurements were performed on a Zetasizer 3000 HS (Malvern Instruments Ltd., Malvern, UK). Data analysis used the non-negatively constrained least-squares (NNLS) method, *via* software provided by Malvern Instruments. The intensity-weighted mean diameter, designated Z_{av}, and the polydispersity index[28,29] were measured at least three times, with replicate measurements always agreeing within 10%. The average of these measurements is reported. The polydispersity index is a measure of the broadness of the size distribution and ranges from 0 to 1; 0.08 or less is effectively monodisperse, and 0.7 or greater is very polydisperse.

Analysis of Surface Charge of Particles (Zeta Potential). The zeta potential[30] was determined using the Zetasizer 3000 HS (Malvern Instruments Ltd., Malvern, UK). Five measurements were taken, which always agreed within 10% of each other, and the average of these five measurements is reported. The zeta potential is the electric potential at the shear plane boundary between ions associated closely enough with the particle to move with it and bulk solution ions which do not. Values were derived from the electrophoretic mobility of the particles using the Smoluchnowski approximation[30] *via* software provided by Malvern Instruments.

Determination of Secondary Structure by Circular Dichroism (CD). A volume of 250 μL of peptide at 1 mg/mL in PBS was scanned through wavelengths of 200−250 nm using a Jobin Yvon CD6 instrument and a path length of 0.1 cm. The results were recorded as molar ellipticity (with PBS background-subtracted) against wavelength. Secondary structure was inferred from comparisons with model structures.[31]

Analytical Ultracentrifugation. Sedimentation velocity experiments were performed on the fusogenic peptide at 50, 250, and 700 μg/mL in modified PBS (139 mM NaCl, 3.6 mM KH_2PO_4, 23.6 mM Na_2HPO_4, 2.6 mM KCl, 10% D_2O, pH 7.3). Experiments were performed at 50k rpm and 20 °C, using Beckman XLI centrifuges equipped with an AnTi60 rotor and 1.2 mm two-channel Epon-filled centerpieces. Radial absorbance data were collected in continuous scanning mode with 0.003 cm increments at 230 nm (50 μg/mL) or 295 nm (250 and 700 μg/mL) at 5 min intervals for a total of 80 scans without averaging. Varying wavelengths were chosen for the different concentrations to optimize absorbance data collection with respect to the dynamic range of the instrument. A partial specific volume for the peptide ($\bar{v}$) of 0.7819 cm^3/g, buffer density of 1.019 g/cm^3, and buffer viscosity of 1.028 cP were calculated using SEDNTERP.[32] Sedimentation boundaries and equilibrium curves were fit using SEDPHAT[33] and the embedded algorithm for translation of sedimentation coefficients to molecular mass. Distributions of molecular mass were calculated over 100 mass increments between 0.3 and 50 kDa; resulting distributions were smoothed by maximum entropy regularisation[34] to provide a mass profile at 95% confidence interval.

Sedimentation equilibrium data were collected for the fusogenic peptide at 1 mg/mL at 35k and 50k rpm and at a wavelength of 300 nm. Data were collected at 4 h intervals using a radial step size of 0.001 cm and averaging over 10 scans until the sample reached equilibrium (*i.e.*, successive data curves were indistinguishable) at ~24 h. Sedimentation equilibrium data were combined with velocity data for all concentrations and fit globally to a single molecular mass using SEDPHAT. Molecular mass and sedimentation coefficient errors are quoted at 95% confidence interval and were estimated by globally refitting the data after each of 1000 Monte Carlo iterations in which Gaussian-random noise is added to the data.

Amino Acid Analysis. Amino acid analysis was performed by Dr. Peter Sharratt (Department of Biochemistry, Cambridge, UK) by gas phase hydrolysis of the peptide samples using norleucine as the internal standard, followed by ion exchange separation (sodium system) and detection with ninhydrin.

Cell Lines. The T-24 cell line (European Collection of Cell Cultures, Salisbury, UK) is an adherent line originally derived from a human bladder carcinoma. It was maintained under mycoplasma-free conditions in Dulbecco's modified Eagle's medium (DMEM) supplemented with 10% heat-inactivated fetal calf serum, 2 mM glutamine, and 1× nonessential amino acids (Invitrogen, Renfrewshire, UK), referred to as culture medium. The U2-OS cell line (American Type Culture Collection, Middlesex, UK) is an adherent line originally derived from a human osteosarcoma. It was maintained using McCoys 5A medium, with supplements as above.

Electron Microscopy. Peptide particles were formed by incubating biotinylated K_{16}-molossin at 15 μg/mL with the fusogenic peptide at 10 μg/mL in DMEM (without supplements). After 30 min at room temperature, streptavidin−gold (Agar Scientific, Stansted, UK) (10 nm gold particles) was added to a final dilution of 1 in 300 of the stock solution supplied. The gold-labeled particles were added to cells after a further 10 min incubation at room temperature.

The T-24 cells were seeded into 12-well plates at 2×10^5 cells per well, each well containing a sterile 16 mm diameter glass coverslip. The cells were incubated overnight at 37 °C in 5% CO_2/95% air. The culture medium was then removed, the cells were washed once with DMEM without supplements, and 0.75 mL of the gold-labeled peptide particles was added to each well. After 4 h at 37 °C in 5% CO_2/95% air, the solution was removed and 1 mL of ice-cold 2.5% glutaraldehyde in 0.13 M phosphate buffer (pH 7.3) was added to each well. After 2 h at 4 °C, the glutaraldehyde was removed and replaced with 1 mL of ice-cold 0.25 M sucrose in 0.07 M phosphate buffer pH 7.3, and the plate was stored at 4 °C until processing.

The cells were postfixed in 1% osmium tetroxide for 30 min followed by dehydration with 10% ethanol for 10 min, 70% ethanol for 15 min, and 100% ethanol for 15 min (3 times). The coverslip was then fixed onto a glass slide, covered with embedding resin (medium hardness) (TAAB, Reading, UK), and left for 2 h at room temperature. A TAAB embedding capsule was filled with resin, inverted over the coverslip, and placed in an embedding oven at 70 °C for 24 h to polymerize. The embedding capsule was then snapped off, removing the layer of cells from the coverslip.

Ultrathin sections (0.75−2 μm) were cut using a Leica Ultracut machine (Leica Microsystems, Milton Keynes, UK). They were placed on 200 mesh Guilder Grids (EM Technologies Ltd., Ashford, UK) with a support film of 0.5% Pioloform (Agar Scientific Ltd.) in chloroform. The grids were stained with uranyl acetate and lead citrate and viewed on a Hitachi H7600 transmission electron microscope (Hitachi, Wokingham, UK).

Apoptosis Assay. U2-OS cells were seeded into 96-well plates using 0.2 mL at 5×10^4 cells/mL per well and incubated overnight at 37 °C in 5% CO_2/95% air. The following day the cells were washed once with PBS and 100 μL of peptide was added in McCoys 5A medium without supplements. This was incubated for 4 h at 37 °C as above, and then 100 μL of Apo-ONE homogenous caspase-3/7 assay substrate (Promega, Madison, WI) was added. The plate was then covered in foil and placed on a rocker at room temperature for 1 h. Fluorescence was measured using a Beckman Coulter plate reader.

Surface Modification of Peptide Particles. Peptide particles were formed in 20 mM Hepes, pH 7.8, using the K_{16} peptide at 15 μg/mL (3.7 μM) and the fusogenic peptide at 10 μg/mL (4.1 μM). After 30 min at room temperature, the appropriate volume of a copolymer of *N*-(2-hydroxypropyl)methacrylamide and *N*-methacrylated glycylglycine 4-nitrophenol ester (HPMA) (at 50 mg/mL in 20 mM Hepes, pH 7.8) (a kind gift from Dr. Simon Briggs and Professor Len Seymour, Department of Clinical Pharmacology, University of Oxford, England) was added to achieve final concentrations of 0.1−0.5 mg/mL. The HPMA has a molecular weight of 21 500 Da, a composition of 10.3 parts of the glycylglycine nitrophenol ester moiety to 89.7 parts of the hydroxypropyl methacrylamide moiety, with an average of 13.8 reactive nitrophenol groups per molecule.

Acknowledgment. We thank E. Matthews (Yale University) for helpful discussion of the sedimentation data, C. O'Brien (University of Melbourne) for assistance with sample preparation of the fusogenic peptide, W. Gratzer (King's College London) for assistance with the CD data, and K. Brady (King's College London) for his contribution to the microscopy work. This work was supported in part by the Rosetrees Trust.

Supporting Information Available: Supporting table establishes the stoichiometry of nanoparticle formation by forming nanoparticles at various K_{16}:fusogenic peptide ratios, sedimenting the particles by centrifugation and performing amino acid analyses on the supernatant. Supporting Figure 1 shows the Z_{av} of nanoparticles formed at different K_{16}:fusogenic peptide ratios. Supporting Figure 2 demonstrates second round particle formation when fresh fusogenic peptide is added to nanoparticles formed with an excess of K_{16} and shows subsequent merger of particles. It also demonstrates the importance for particle formation of the local concentrations of fusogenic peptide. This material is available free of charge *via* the Internet at http://pubs.acs.org.

REFERENCES AND NOTES

1. Shevchenko, E. V.; Talapin, D. V.; Kotov, N. A.; O'Brien, S.; Murray, C. B. Structural diversity in binary nanoparticle superlattices. *Nature* **2006**, *439*, 55–59.
2. Percec, V.; Dulcey, A. E.; Balagurusamy, V. S.; Miura, Y.; Smidrkal, J.; Peterca, M.; Nummelin, S.; Edlund, U.; Hudson, S. D.; Heiney, P.A.; *et al.* Self-assembly of amphiphilic dendritic dipeptides into helical pores. *Nature* **2004**, *430*, 764–768.
3. O'Reilly, R. K. Spherical polymer micelles: nanosized reaction vessels? *Philos. Trans. A* **2007**, *365*, 2863–2878.
4. Bognolo, G. The use of surface-active agents in the preparation and assembly of quantum-sized nanoparticles. *Adv. Colloid Interface Sci.* **2003**, *106*, 169–181.
5. Wright, E. R.; Conticello, V. P. Self-assembly of block copolymers derived from elastin-mimetic polypeptide sequences. *Adv. Drug Delivery Rev.* **2002**, *54*, 1057–1073.
6. Kalsin, A. M.; Fialkowski, M.; Paszewski, M.; Smoukov, S. K.; Bishop, K. J.; Grzybowski, B. A. Electrostatic self-assembly of binary nanoparticle crystals with a diamond-like lattice. *Science* **2006**, *312*, 420–424.
7. Kalsin, A. M.; Grzybowski, B. A. Controlling the growth of "ionic" nanoparticle supracrystals. *Nano Lett.* **2007**, *7*, 1018–1021.
8. Bishop, K. J.; Grzybowski, B. A. "Nanoions": fundamental properties and analytical applications of charged nanoparticles. *ChemPhysChem* **2007**, *8*, 2171–2176.
9. Yang, Y.; Khoe, U.; Wang, X.; Akihiro, H.; Hidenori, Y.; Zhang, S. Designer self-assembling peptide nanomaterials. *Nano Today* **2009**, *4*, 193–210.
10. Parker, A. L.; Collins, L.; Zhang, X.; Fabre, J. W. Exploration of peptide motifs for potent non-viral gene delivery highly selective for dividing cells. *J. Gene Med.* **2005**, *7*, 1545–1554.
11. Lear, J. D.; DeGrado, W. F. Membrane binding and conformational properties of peptides representing the

NH2 terminus of influenza HA-2. *J. Biol. Chem.* **1987**, *262*, 6500–6505.
12. Skehel, J. J.; Cross, K.; Steinhauer, D.; Wiley, D. C. Influenza fusion peptides. *Biochem. Soc. Trans.* **2001**, *29*, 623–626.
13. Gottschalk, S.; Sparrow, J. T.; Hauer, J.; Mims, M. P.; Leland, F. E.; Woo, S. L.; Smith, L. C. A novel DNA−peptide complex for efficient gene transfer and expression in mammalian cells. *Gene Ther.* **1996**, *3*, 448–457.
14. Fabre, J. W.; Collins, L. Synthetic peptides as non-viral DNA vectors. *Curr. Gene Ther.* **2006**, *6*, 459–480.
15. Chauhan, A.; Tikoo, A.; Kapur, A. K.; Singh, M. The taming of the cell penetrating domain of the HIV Tat: myths and realities. *J. Controlled Release* **2007**, *117*, 148–162.
16. Futaki, S.; Suzuki, T.; Ohashi, W.; Yagami, T.; Tanaka, S.; Ueda, K.; Sugiura, Y. Arginine-rich peptides. An abundant source of membrane-permeable peptides having potential as carriers for intracellular protein delivery. *J. Biol. Chem.* **2001**, *276*, 5836–5840.
17. Mäe, M.; Langel, U. Cell-penetrating peptides as vectors for peptide, protein and oligonucleotide delivery. *Curr. Opin. Pharmacol.* **2006**, *6*, 509–514.
18. Zorko, M.; Langel, U. Cell-penetrating peptides: mechanism and kinetics of cargo delivery. *Adv. Drug Delivery Rev.* **2005**, *57*, 529–545.
19. Chen, L.; Harrison, S. D. Cell-penetrating peptides in drug development: enabling intracellular targets. *Biochem. Soc. Trans.* **2007**, *35*, 821–825.
20. Wadia, J. S.; Stan, R. V.; Dowdy, S. F. Transducible TAT-HA fusogenic peptide enhances escape of TAT-fusion proteins after lipid raft macropinocytosis. *Nat. Med.* **2004**, *10*, 310–315.
21. Nakase, I.; Niwa, M.; Takeuchi, T.; Sonomura, K.; Kawabata, N.; Koike, Y.; Takehashi, M.; Tanaka, S.; Ueda, K.; Simpson, J. C.; *et al.* Cellular uptake of arginine-rich peptides: roles for macropinocytosis and actin rearrangement. *Mol. Ther.* **2004**, *10*, 1011–1022.
22. Ziady, A. G.; Perales, J. C.; Ferkol, T.; Gerken, T.; Beegen, H.; Perlmutter, D. H.; Davis, P. B. Gene transfer into hepatoma cell lines *via* the serpin enzyme complex receptor. *Am. J. Physiol.* **1997**, *273*, G545–G552.
23. Scarborough, R. M.; Rose, J. W.; Naughton, M. A.; Phillips, D. R.; Nannizzi, L.; Arfsten, A.; Campbell, A. M.; Charo, I. F. Characterization of the integrin specificities of disintegrins isolated from American pit viper venoms. *J. Biol. Chem.* **1993**, *268*, 1058–1065.
24. Shewring, L.; Collins, L.; Lightman, S. L.; Hart, S.; Gustafsson, K.; Fabre, J. W. A nonviral vector system for efficient gene transfer to corneal endothelial cells *via* membrane integrins. *Transplantation* **1997**, *64*, 763–769.
25. Greenspoon, N.; Hershkoviz, R.; Alon, R.; Varon, D.; Shenkman, B.; Marx, G.; Federman, S.; Kapustina, G.; Lider, O. Structural analysis of integrin recognition and the inhibition of integrin-mediated cell functions by novel nonpeptidic surrogates of the Arg-Gly-Asp sequence. *Biochemistry* **1993**, *32*, 1001–1008.
26. Nissinen, M.; Vuolteenaho, R.; Boot-Handford, R.; Kallunki, P.; Tryggvason, K. Primary structure of the human laminin A chain. Limited expression in human tissues. *Biochem. J.* **1991**, *276*, 369–379.
27. Chen, Y. P.; Sharma, S. K.; Ramsey, T. M.; Jiang, L.; Martin, M. S.; Baker, K.; Adams, P. D.; Bair, K. W.; Kaelin, W. G. Selective killing of transformed cells by cyclin/cyclin-dependent kinase 2 antagonists. *Proc. Natl. Acad. Sci. U.S.A.* **1999**, *96*, 4325–4329.
28. International Standard ISO13321. Methods for Determination of Particle Size Distribution Part 8: Photon Correlation Spectroscopy, International Organisation for Standardisation, 1996.
29. Cornell, B. A.; Fletcher, G. C.; Middlehurst, J.; Separovic, F. The temperature dependence of the size of phospholipid vesicles. *Biochim. Biophys. Acta* **1981**, *642*, 375–380.
30. Hunter, R. J. *Zeta Potential in Colloid Science*; Academic Press: London, 1981.
31. Gratzer, W. B.; Beaven, G. H. Optical spectroscopy in techniques in the life sciences. *Protein and Enzyme Biochemistry*; Elsevier: Amsterdam, 1984; pp 1−47.
32. Hayes, D. B.; Laue, T.; Philo, J. *SEDNTERP: Interpretation of Sedimentation Data*, version v1.09; University of New Hampshire, 2003,; http://www.rasmb.bbri.org.
33. Schuck, P.; Rossmanith, P. Determination of the sedimentation coefficient distribution by least-squares boundary modeling. *Biopolymers* **2000**, *54*, 328–341.
34. Schuck, P. Size distribution analysis of macromolecules by sedimentation velocity ultracentrifugation and Lamm equation modeling. *Biophys. J.* **2000**, *78*, 1606–1619.
35. Humphrey, W.; Dalke, A.; Schulten, K. VMD—Visual Molecular Dynamics. *J. Mol. Graphics* **1996**, *14*, 33–38.
36. Phillips, J. C.; Braun, R.; Wang, W.; Gumbart, J.; Tajkhorshid, E.; Villa, E.; Chipot, C.; Skeel, R. D.; Kalé, L.; Schulten, K. Scalable molecular dynamics with NAMD. *J. Comput. Chem.* **2005**, *26*, 1781–1802.
37. Straume, M.; Johnson, M. L. Analysis of residuals—criteria for determining goodness-of-fit. *Methods Enzymol.* **1992**, *210*, 87–105.